The Mach Reflection of Shock Waves at Nearly Glancing Incidence*†

C. H. FLETCHER, *Department of Aeronautical Engineering,*
A. H. TAUB, *Department of Mathematics,*
AND
WALKER BLEAKNEY,‡ *Department of Physics,*
University of Illinois, Urbana, Illinois

INTRODUCTION

AN experimental investigation of the interaction of a plane shock wave in air with a plane rigid wall reveals that this reflection phenomenon takes at least the two forms which are illustrated in Fig. 1: (a) regular reflection in which the original or incident shock is followed by a reflected shock which joins the incident shock wave at the wall and (b) Mach reflection in which the reflected shock meets the incident shock at a triple point (or line) which is some distance from the wall and is joined to it by a third shock wave (usually curved) called the Mach shock. For the case of a shock wave of any specified (finite) strength, Mach reflection will always occur if the incidence is sufficiently near glancing and regular reflection will occur if the incidence of the shock wave on the wall is sufficiently near head-on.

In an earlier paper[1] this problem was discussed principally from a theoretical viewpoint. A complete mathematical solution to the problem of Mach reflection is very difficult because of the nonlinear nature of the problem and the fact that the location and strengths of the reflected and Mach shocks which are to be determined by the analysis also specify the boundary conditions for the flow. Nevertheless, various assumptions can be made which do not affect the nonlinear character of the problem but treat the conditions in the vicinity of the triple point for Mach reflection or, for regular reflection, the conditions near the intersection of the incident and reflected shocks. These treatments are fundamentally local in character and are made in detail in reference **1.**

The problem is essentially a two-dimensional one, and it is usual to consider the configuration of the intersections of the shock waves with a plane which is perpendicular to the wall and to the incident shock. In considering these local problems it is usually convenient to choose the origin at the point in question and reduce it to rest. When this is done, the conditions for regular reflection are that the incident shock wave is stationary in a uniform flow parallel to the wall and the reflected shock is stationary and such that the flow behind it is parallel to the wall. In this case, the flow approaching the incident shock is supersonic and the flow between the incident and reflected shocks is supersonic, but that behind the reflected shock may be either supersonic or subsonic, depending on how nearly the incidence is head-on and how strong the incident shock wave is. In the case that this flow is supersonic the reflected shock is straight and of uniform strength at least in the neighborhood of the origin, since small signals originating at the corner or along the wall between the corner and the origin propagate with sound velocity relative to the gas; hence, they are unable to reach the origin. The region between the origin and the first signal is one of uniform conditions and, of course, grows as the corner recedes. These signals from the corner propagate in all directions in the gas and reach the reflected shock somewhere along its length. In the region where these signals reach the reflected shock, it is curved. When the flow behind the reflected shock is subsonic, these signals affect the whole length of the reflected shock and it is curved over its whole length. A similarity might be pointed out between these two cases for the reflected shock and those for a nose shock attached to a finite wedge, where the shoulder of the wedge serves as the source of signals which render the nose shock curved.

The application of the uniformity condition and the above boundary conditions for the shock configuration leads to a double-valued function which expresses the location of the reflected shock as a function of the location of the incident shock for a given shock strength. One branch of this function agrees with experiments as indicated in reference 1.

It is shown further in reference 1 that for any shock strength there exists a range of angles of incidence where no reflected shock can be introduced which will make the flow behind it parallel to the wall. This range includes glancing incidence. Thus, the theory and experiment agree qualitatively in indicating that at least two types of reflection process occur.

A theoretical treatment of Mach reflection is more difficult, since there is an added variable quantity in the

* Parts of this paper were submitted by the first author in partial fulfillment of the requirements for the degree of Doctor of Philosophy at Princeton University.

† This work was supported in part by the ONR. Contract N6ori-105 Task II with Princeton University.

‡ On leave from Princeton University.

[1] Walker Bleakney and A. H. Taub, Revs. Modern Phys. **21**, 584–605 (1949).

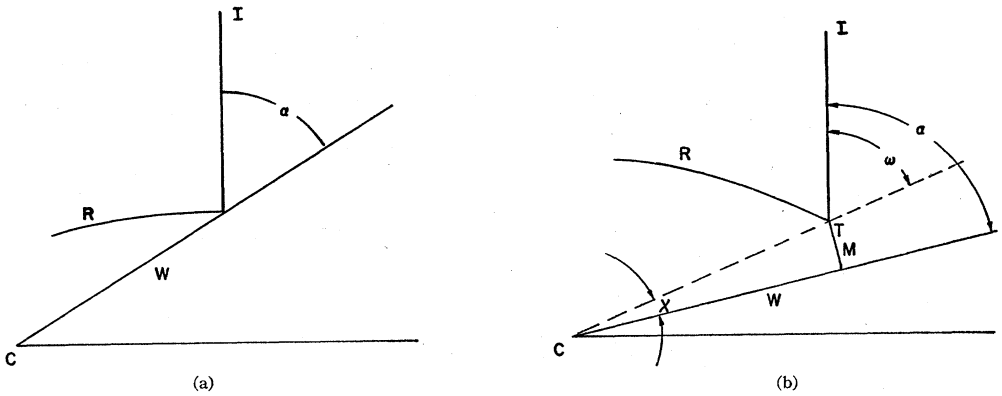

FIG. 1. Diagram of the resultant interaction when a plane shock wave (traveling to the right in these diagrams) strikes an inclined wall, W. The point of first impact, C, is usually called the corner of the wall. (a) Regular reflection in which the incident shock I and the reflected shock R meet at the wall. (b) Mach reflection in which the incident shock I and the reflected shock R meet at the triple point T which is joined to the wall by the Mach shock M. The angles α, ω, and χ are defined according to these diagrams.

distance of the triple point from the wall. One point of attack originates with a dimensional argument which indicates that, when viscosity and heat conductivity are neglected, there is no intrinsic length in the problem (differential equations, shock conditions, and boundary conditions) and the problem may be stated in terms of the independent variables x/t, y/t alone instead of x, y, t. In this notation x and y are rectilinear coordinates in space and t is the time measured from the instant the incident shock wave struck the corner.

On this basis, the triple point travels along a straight line through the corner and the shock configuration grows with the corner (or the triple point) as a center of similitude. Using this as a basis, Fig. 1 shows the configuration with a convenient notation for the angles. The angle α is that between the incident shock wave and the wall, and χ is the angle which the (straight) path of the triple point makes with the wall. The angle ω is between the incident shock and the path of the triple point, and the angles locating the other shock waves are measured from this line. The triple point moves along its path much as the intersection of the incident and reflected shocks moves along the wall in regular reflection, but the conditions on the flow behind the reflected shock do not constrain its direction as in the case of regular reflection.

When, as in the treatment of regular reflection, a coordinate system is chosen in which the triple point is at rest, the angle between the incident shock and the flow impinging on it is ω. The conditions behind the reflected shock are now affected by the presence of the Mach shock; and the reflected and Mach shocks are, in general, curved. If the curvature of these shocks is finite, consideration of a small enough region in the neighborhood of the triple point should permit them to be treated as straight segments; and the configuration involved is that of Fig. 2. The regions 1, 2, 3, and 4 of this figure are all considered to be uniform; a more general problem involves consideration of angular phenomena centered at the triple point. The conditions on the location and strength of the reflected and Mach shocks is that the pressure be the same in regions 3 and 4 and that the flow velocities in these regions be parallel. On the basis of these assumptions, the location and strength of the reflected and Mach shocks may be calculated as a function of the angle ω and the strength of the incident shock.

The analysis[1] indicates that for any specified initial shock strength there is a range of values of ω near 90° where no three shock configuration with three non-zero shocks can satisfy the conditions stipulated above. For each value of ω within this range there is a solution in which the reflected shock is infinitesimal and the incident and Mach shocks lie along the same line. This solution of the three-shock conditions has been called a "trivial" three-shock solution[1] because there is in reality only one shock present. In the case of the Mach reflection of a shock at a wall, this infinitesimal reflected shock may be considered to be a sound signal originating at the corner of the wall and traveling with sonic velocity relative to the flow behind the incident shock; thus, the particular value of ω for this condition may be calculated.

As explained in reference 1, the measurements of angles in Mach and regular reflection by Smith[2] and others show agreement for the case of regular reflection; but in the case of Mach reflection, especially for weak shocks, there are measured values of ω which lie well within the forbidden range mentioned above. This is not a case of experimental inaccuracy, since the incident shock is straight and its angle with the wall is easily measured, and the angle χ can be determined accurately as well. The experimental justification for assuming that the similitude property holds is also apparently quite

[2] L. G. Smith, "Photographic investigations of the reflection of plane shocks in air," OSRD No. 6271 (1945).

firm. Theoretical and experimental investigations[3] indicate that no reasonably placed angular variations of the Prandtl-Meyer type can resolve this discrepancy.

The mathematical problem in the case of nearly glancing incidence may be simplified by linearizing both the differential equation and the boundary condition. This procedure involves assuming a zero-order solution and determining a first-order one in terms of it. The only zero-order solution which can be used is a trivial one in which the reflected wave is assumed to be a sound signal and hence of zero strength. In the following we will discuss three different treatments of this problem made by three different workers, and their results will be compared with experiment.

PSEUDO-STATIONARY FLOW

The motion of a gas when the effects of viscosity and heat conduction may be neglected is described by the following set of differential equations:

$$(d\rho/dt)+\rho\partial u^i/\partial x^i=0, \tag{1}$$

$$\rho du^i/dt=-\partial p/\partial x^i, \tag{2}$$

$$dS/dt=0, \tag{3}$$

where summation over the index i is implied by its repetition in a term. The symbols S, p, ρ represent, respectively, the specific entropy, pressure, and density in the gas; the x^i are the coordinates in any convenient cartesian system and the u^i are the components of the velocity field in the fluid. The derivative d/dt is the material derivative which indicates the variation on following a particle of the fluid. When suitable conditions are prescribed at the boundaries of a region, these equations may, in principle, be solved to give a complete description of the properties of the fluid within this region. The boundaries involved may be walls or similar physical elements and they may include shock waves or other discontinuity surfaces. The conditions at the boundaries may be given by the Rankine-Hugoniot equations which relate the properties across a shock wave, or they may specify that the normal component of the difference of the velocities of the gas and the wall be zero at the wall.

A simplification may be achieved for those problems where the boundaries are given by relations of the form

$$x^i=tf_{(k)}{}^i(s^1, s^2), \tag{4}$$

where the subscript (k) indicates the boundary in question and the parameters s^1, s^2 describe the surface when $t=1$. The substitution $a^i=x^i/t$ leads to the following form of the differential operators in Eqs. (1) to (3):

$$dg/dt=(1/t)(u^i-a^i)g_{,i}=U^ig_{,i}/t, \tag{5}$$

$$\partial g/\partial x^i=g_{,i}/t, \tag{6}$$

[3] V. Bargmann and D. Montgomery, "Prandtl-Meyer zones in Mach reflection," OSRD No. 5011. See also reference 2.

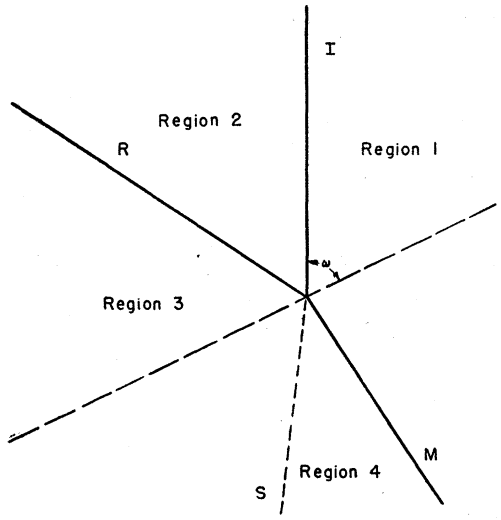

FIG. 2. Diagram of the idealized conditions in the vicinity of the triple point in Mach reflection. The three shock waves I, R, and M are considered to be straight (planar). Under these conditions the gas in region 3 (behind both I and R) is at the same pressure as that in region 4 (behind M), but their densities and velocities differ. This gives rise to the slipstream S shown with the shorter dashes. The other dashed line is the path of the triple point shown in Fig. 1(b).

where $g(x^1/t, x^2/t, x^3/t)$ is any function into which the coordinates and time enter in the manner indicated and the derivative $\partial g/\partial a^i$ has been written $g_{,i}$. The symbol U^i is defined in Eq. (5).

When this substitution is introduced into Eqs. (1) to (3), the differential equations become

$$U^i\rho_{,i}+\rho U_{,i}{}^i+2\rho=0, \tag{7}$$

$$\rho U^i+\rho U^jU_{,j}{}^i=-p_{,i}, \tag{8}$$

$$U^iS_{,i}=0, \tag{9}$$

and the boundaries take the form $a^i=f_{(k)}{}^i(s^1, s^2)$. A flow which meets these requirements may be called pseudo-stationary, since the time does not appear explicitly in the formulation.

An investigation of the conditions at the boundaries will be made only for the case that all the flow vectors are parallel to a plane and that an analysis of conditions in this plane describe the whole field. This type of two-dimensional flow is of importance in the Mach reflection problem, and a similar investigation of the conditions for other types of flow may be made. This restriction makes only a few changes in the relations written above; the range of the index i is now $i=1, 2$, and there is only one parameter s in the relations which specify the boundaries.

Consider first the case that the boundary is a shock wave; the Rankine-Hugoniot equations concern local conditions at each point of the shock and involve the orientation of the shock front, the components of the velocity of the fluid relative to the shock, and the pressure on the two sides of the shock. Let $\lambda_{(k)}{}^i(s)$ be the

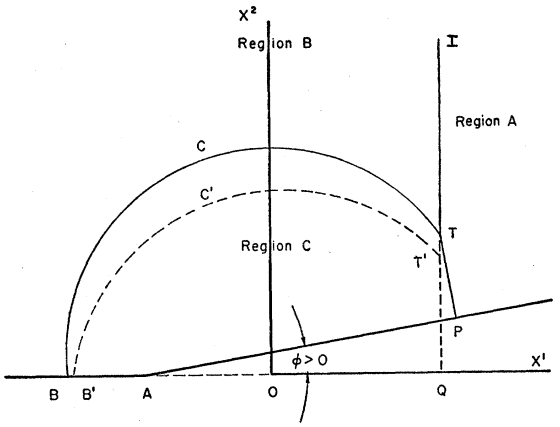

FIG. 3. The interaction of a weak incident shock I with a concave corner (nearly glancing incidence). The actual reflected shock is indicated by the full line BCT and the actual Mach shock by the full line TP. Region A is the undisturbed gas ahead of the incident shock. Region B has been affected by the incident shock, but no signal from the wall has reached it. Region C has been affected both by the incident shock and the presence of the wall. The dashed boundaries $B'C'T'$ and $T'Q$ are the zero-order boundaries for Bargmann's approximation treatment.

components of a unit vector normal to the shock (k) at the point specified by s. The normal vector will be drawn into the *region 1* which is *ahead* of the shock while *region 2* is *behind* it. This convention serves to identify the italicized terms. The components of a unit vector tangent to the shock (k) will be noted by $\mu_{(k)}{}^i$.

The velocity of a point $x_{(k)}{}^i(s)$ on the shock has components given by

$$dx_{(k)}{}^i/dt=f_{(k)}{}^i(s)=a_{(k)}{}^i \tag{10}$$

from Eq. (4). The tangential components of the flow relative to the shock must be equal on the two sides of the shock:

$$\begin{aligned}(u_1{}^i-a^i)\mu^i&=(u_2{}^i-a^i)\mu^i,\\ U_1{}^i\mu^i&=U_2{}^i\mu^i.\end{aligned} \tag{11}$$

The normal components of the flow relative to the shock are related to the pressure ratio across the shock according to

$$\begin{aligned}p_2/p_1&=[2\gamma\sigma_1{}^2-(\gamma-1)]/(\gamma+1)\\ &=(\gamma+1)/[2\gamma\sigma_2{}^2-(\gamma-1)],\end{aligned} \tag{12}$$

where σ is the ratio of the normal component of the flow relative to the shock to the speed of sound c in the gas and

$$\sigma_\alpha=(u_\alpha{}^i-a^i)\lambda^i/c_\alpha=U_\alpha{}^i\lambda^i/c_\alpha,\quad \alpha=1,2. \tag{13}$$

Other forms of the Rankine-Hugoniot relations give

$$\rho_2/\rho_1=(\gamma+1)\sigma_1{}^2/[(\gamma-1)\sigma_1{}^2+2], \tag{14}$$

$$U_2{}^i\lambda^i-U_1{}^i\lambda^i=2c_1(1-\sigma_1{}^2)/(\gamma+1)\sigma_1. \tag{15}$$

If the boundary is a wall, the condition of the flow may be stated in the form that along the wall

$$U^i\lambda^i=0. \tag{16}$$

LINEARIZATION OF THE GLANCING INCIDENCE PROBLEM

In the limit of truly glancing incidence ($\alpha=90°$) the original shock will be unaffected and there will be at most a sound signal emanating from the interaction of the incident shock and the corner and progressing into the gas behind the incident shock. This situation is illustrated by the dash lines of Fig. 3 and constitutes the zero-order boundary for this treatment of the problem. The actual situation when the wall makes an angle φ with the normal to the shock is illustrated by the solid lines of Fig. 3.

The coordinate system which is most convenient for discussing this problem is at rest relative to the gas behind the incident shock. Relative to this coordinate system, the incident shock moves to the right and the corner moves to the left. The x^1 axis is perpendicular to the incident shock front and is positive in the direction that this shock is moving. The x^2 axis coincided with the incident shock at time $t=0$ when the incident shock struck the corner.

As mentioned in the introduction, experimental evidence indicates that the Mach configuration grows in time with the corner as a center of similitude and consists of the three regions enclosed by the solid lines of Fig. 3. Region A contains gas not yet affected by the incident shock, region B contains the gas which has been passed over by the incident shock but has not yet been affected by the presence of the wall, and region C contains the gas affected by both the incident shock and the wall. The properties of the gas in each region will be identified by a subscript which corresponds to this identification of the regions except for the properties in region C, which is that of interest, where no subscripts will be used.

In the coordinate system chosen (Fig. 3), it is convenient to choose the units of distance and time so that the velocity of sound and the density in the gas of region B have the value unity. In these units the pressure there will be $1/\gamma$; the shock will move to the right with velocity σ_s, and the velocity of the corner and of the gas in region A will be directed to the left and of magnitude D. The other properties of the gas in region A depend on the strength of the incident shock which is conveniently measured by the σ_s defined above. In terms of this parameter,

$$D=2(1-\sigma_s{}^2)/(\gamma+1)\sigma_s. \tag{17}$$

The pressure is given by the Rankine-Hugoniot equation,

$$p_A=[2\gamma\sigma_s{}^2-(\gamma-1)]/\gamma(\gamma+1), \tag{18}$$

the density by

$$\rho_A=(\gamma+1)\sigma_s{}^2/[(\gamma-1)\sigma_s{}^2+2], \tag{19}$$

and the velocity of sound by

$$c_A{}^2=[(\gamma-1)\sigma_s{}^2+2][2\gamma\sigma_s{}^2-(\gamma-1)]/(\gamma+1)^2\sigma_s{}^2. \tag{20}$$

The relation defining the wall AP is of the form,

$$x^2=\delta(x^1+Dt);\quad x^1\gtrless -Dt, \tag{21}$$

where δ is the tangent of the angle φ. The undisturbed incident shock is given by the relation $x^1=\sigma_s t$ and the perturbed portion TP by a relation of the form,

$$x^1=t[\sigma_s+\delta f_{(1)}(x^2/t)], \tag{22}$$

which reduces to that above when $\delta=0$. The curve BCT would be a circular arc of unit radius if the perturbation were infinitesimal, since it would then be the locus of a sound signal generated in the gas of region B by the corner and spreading with center 0. In the approximation involved here this curve may be given in polar coordinates by $r=[1+\delta f_{(2)}(\theta)]t$. These boundaries are all of the form required for the pseudo-stationary formulation to apply.

In pseudo-stationary form the boundaries may be written

$$BA:\quad a^2=0; \tag{23}$$

$$AP:\quad a^2=\delta(a^1+D); \tag{24}$$

$$PT:\quad a^1=\sigma_s+\delta f_{(1)}(a^2); \tag{25}$$

$$TCB:\quad a^1=[1+\delta f_{(2)}(\theta)]\cos\theta, \tag{26}$$

$$a^2=[1+\delta f_{(2)}(\theta)]\sin\theta. \tag{27}$$

Inside region C the properties of the flow will be only slightly different from those in region B for sufficiently small δ. The components of the velocity field in region C are of the order of δ, and the pressure and density in this region may be given by

$$p=(1+\Delta p)/\gamma, \tag{28}$$

$$\rho=(1+\Delta\rho), \tag{29}$$

where $\Delta\rho$ and Δp are of the order δ.

The differential Eqs. (7), (8), and (9) may be linearized by neglecting orders of δ higher than the first and assuming that the derivatives of small quantities are small; the result is

$$u_{,i}{}^i-a^i\Delta\rho_{,i}=0, \tag{30}$$

$$a^iu_{,j}{}^i=\Delta p_{,i}/\gamma, \tag{31}$$

$$a^iS_{,i}=0. \tag{32}$$

The boundaries of region C have been given in the form,

$$a^i=a_0{}^i+\delta a_1{}^i, \tag{33}$$

where the dependence on δ is shown explicitly and $a_0{}^i$ and $a_1{}^i$ depend on a suitable parameter. All of the properties which characterize the flow in regions A and B are constants, whereas at the boundaries in region C they may be written in the form,

$$\psi(a^i)=\psi_0+\delta\psi_1(a^i), \tag{34}$$

where ψ_0 is a constant. Now, we have $\psi_1(a^i)=\psi_1(a_0{}^i)$, since terms in powers of δ higher than the first are to be neglected. Hence, the boundary conditions are to hold on the zeroth order boundaries of region C which are indicated in Fig. 3 as $B'A$, AQ, QT', and $T'C'B'$.

The boundary conditions along the wall may be written down on reference to Eq. (16):

Along the wall $B'A$:

$$U^2=0=u^2-a^2=u^2. \tag{35}$$

Along the wall AQ: the components of the normal vector are

$$\lambda^1=-\delta,\quad \lambda^2=1,$$

$$U^i\lambda^i=0=-\delta(u^1-a^1)+(u^2-a^2), \tag{36}$$

$$u^2=\delta D.$$

The condition on the derivatives of the pressure along the wall may be determined from those from the velocity by using the equation of motion Eq. (31).

$$\Delta p_{,2}=\gamma a^iu_{,i}{}^2=0, \tag{37}$$

except at the corner where $u_{,1}{}^2$ is not defined. By introducing the limiting process,

$$\lim_{a^2\to 0}\int_{-D-\eta}^{-D+\eta}\Delta p_{,2}da^1$$

$$=-\gamma D[u^2(-D+\eta)-u^2(-D-\eta)]=-\gamma\delta D^2,$$

we may represent the quantity $\Delta p_{,2}$ by a delta-function

$$\Delta p_{,2}=-\delta D^2\gamma[\text{delta-function of } (-D-a^1)]. \tag{38}$$

Along the reflected shock TCB:

$$\mu^1=-\sin\theta+\delta f_{(2)}{}'(\vartheta)\cos\theta,$$

$$\mu^2=\cos\theta+\delta f_{(2)}{}'(\vartheta)\sin\theta,$$

where the prime denotes differentiation with respect to the argument indicated. The requirement that $U_B{}^i\mu^i=U_C{}^i\mu^i$ gives

$$-u^1\sin\theta+u^2\cos\theta=0, \tag{39}$$

since u^1 and u^2 are first order in δ. This must hold along the part $T'C'B'$ of the unit circle. Application of the other Rankine-Hugoniot equations to this boundary gives

$$\Delta p=(4\gamma/[\gamma+1])f_{(2)}\delta=\gamma\Delta\rho, \tag{40}$$

$$u^1\cos\theta+u^2\sin\theta=(4/[\gamma+1])f_{(2)}\delta=a_0{}^1u^1+a_0{}^2u^2. \tag{41}$$

Along the Mach shock TP: $a^1=\sigma_s+\delta f_{(1)}(a^2)$ and the quantities $U_A{}^1=-D-\sigma_s-f_1\delta$ and $U_A{}^2=-a^2$ take the forms indicated. The quantity σ_A defined as in Eq. (13) may be calculated in terms of σ_s using the results of Eqs. (17), (18), (19), and (20). The application of Eqs. (11), (12), (14), and (15) leads to the following relations which must hold along the zeroth order

boundary QT':

$$\Delta p=(4\gamma\sigma_s/[\gamma+1])[f_{(1)}-a^2f_{(1)}']\delta, \tag{42}$$

$$\Delta\rho=\frac{4[2\gamma\sigma_s^2-(\gamma-1)]}{(\gamma+1)\sigma_s[(\gamma-1)\sigma_s^2+2]}[f_{(1)}-a^2f_{(1)}']\delta, \tag{43}$$

$$u^1=\frac{2}{\gamma+1}\frac{(3\gamma-1)\sigma_s^2-(\gamma-3)}{(\gamma-1)\sigma_s^2+2}[f_{(1)}-a^2f_{(1)}']\delta, \tag{44}$$

$$u^2=-D\delta f_{(1)}'. \tag{45}$$

BARGMANN'S SOLUTION

In 1945, V. Bargmann[4] reported a solution of this linearized problem for the case of weak incident shocks. It was assumed that regions B and C of Fig. 3 were uniformly of the same entropy. This approximation is valid when the reflected signal is weak and the curvature of the Mach shock is slight.

When this assumption of isentropy is made, Eq. (32) may be replaced by

$$\Delta p=\gamma\Delta\rho \tag{46}$$

and Δp and $\Delta\rho$ may be eliminated from Eqs. (30), (31), and (46) to give the single relation

$$u_{,i}{}^i-a^ia^iu_{,j}{}^i=0, \tag{47}$$

which must be satisfied by the components u^i. A velocity potential may be introduced according to the relation,

$$u^i=-\delta\Omega_{,i}, \tag{48}$$

where the approximation parameter δ has been introduced explicitly. An integration of the momentum equations (31) leads to the relation,

$$\Delta p=\gamma\delta(\Omega-a^i\Omega_{,i})=\gamma\delta\boldsymbol{\Omega} \tag{49}$$

and

$$\Delta\rho=\delta\boldsymbol{\Omega}, \tag{50}$$

while Ω satisfies the second-order differential equation,

$$\Omega_{,ii}-a^ia^i\Omega_{,ij}=0 \tag{51}$$

The boundary conditions on Ω and its derivatives along the zeroth-order boundaries may be written down by referring to Eqs. (35) to (45):

Along $B'A$:

$$\Omega_{,2}=0. \tag{35'}$$

On AQ:

$$\Omega_{,2}=-D. \tag{36'}$$

On $B'C'T'$:

$$\partial\Omega/\partial\theta=0 \quad \text{or} \quad \Omega=\text{const}, \tag{39'}$$

$$\boldsymbol{\Omega}=(4/[\gamma+1])f_{(2)}, \tag{40'}$$

$$r\partial\Omega/\partial r=(-4/[\gamma+1])f_{(2)}. \tag{41'}$$

On $T'Q$:

$$\boldsymbol{\Omega}=(4\sigma_s/[\gamma+1])(f_{(1)}-a^2f_{(1)}'), \tag{42'}$$

$$\Omega_{,1}=-\frac{2}{\gamma+1}\left[\frac{(3\gamma-1)\sigma_s^2-(\gamma-3)}{(\gamma-1)\sigma_s^2+2}\right](f_{(1)}-a^2f_{(1)}'), \tag{44'}$$

$$\Omega_{,2}=Df_{(1)}'. \tag{45'}$$

Since $\boldsymbol{\Omega}=\Omega-a^i\Omega_{,i}$, Eqs. 40′ and 41′ may be combined to determine that along $B'C'T'$

$$\Omega=0 \tag{52}$$

and

$$f_{(2)}=(\gamma+1)\boldsymbol{\Omega}/4. \tag{53}$$

The quantity $(f_1-a^2f_1')$ may be eliminated between Eqs. (42′) and (44′), and a^1 may be set equal to σ_s along $T'Q$ to give

$$\Omega-\sigma_s\Omega_{,1}-a^2\Omega_{,2}=-2\sigma_s\Omega_{,1}\frac{(\gamma-1)\sigma_s^2+2}{(3\gamma-1)\sigma_s^2-(\gamma-3)} \tag{54}$$

or

$$\Omega-a^2\Omega_{,2}=\Omega_{,1}(\sigma_s-1)\left[1+(1-\sigma_s)\frac{2(\gamma-1)\sigma_s+(\gamma-3)}{(3\gamma-1)\sigma_s^2-(\gamma-3)}\right]; \tag{55}$$

for values of σ_s near 1 the boundary condition along $T'Q$ may be written

$$\Omega-a^2\Omega_{,2}=-(1-\sigma_s)\Omega_{,1}. \tag{56}$$

To determine f_1, Eqs. (44′), (55), and (17) are combined to give

$$\Omega-a^2\Omega_{,2}=D\left[1+\frac{2(\sigma_s^2-1)}{(\gamma-1)\sigma_s^2+2}\right](f_{(1)}-a^2f_{(1)}'), \tag{57}$$

from which

$$f_{(1)}(a^2)=\Omega(\sigma_s, a^2)/D \tag{58}$$

for sufficiently weak incident shocks.

The differential equation may be solved subject to these boundary conditions by introducing the variables

$$k^i=a^i/(1+s), \tag{59}$$

where $(s)^2=1-a^ia^i$, which transforms it into the Laplace equation in these variables. It can be shown that the $\Omega_{,i}$ and $\boldsymbol{\Omega}$ are harmonic in these variables. The solution of the laplace equation may then be obtained by a conformal mapping procedure.

A further condition on the types of solution allowed is that the total kinetic energy in region C be of first or higher order in δ. This condition is given by requiring that $\int\int_C(\Omega_{,1}{}^2+\Omega_{,2}{}^2)da^1da^2$ is finite.

A summary of Bargmann's results for an incident shock of strength σ_s is as follows:

$a^i=x^i/t$; $D=2(1-\sigma_s^2)/(\gamma+1)\sigma_s$; $p_B=1/\gamma$; $\rho_B=1$; $c_B=1$; $u^i=-\delta\Omega_{,i}$; $p=p_B(1+\gamma\delta\boldsymbol{\Omega})$, $\rho=\rho_B(1+\delta\boldsymbol{\Omega})$; $\boldsymbol{\Omega}=\Omega-a^i\Omega_{,i}=\Omega-r\partial\Omega/\partial r$.

[4] V. Bargmann, "On nearly glancing reflection of shocks," AMP Report 108.2R NDRC (1945).

The reflected shock is given by

$$r=1+\delta f_{(2)}(\theta),$$
$$f_2=-\tfrac{1}{4}(\gamma+1)\partial\Omega/\partial r \quad (r=1).$$

The Mach shock is given by

$$a^1=\sigma_s+\delta f_{(1)}(a^2),$$
$$f_1=\Omega(\sigma_s, a^2)/D,$$
$$\Omega=(D/\pi)(f_{(d)}-mf_{(-b)}),$$
$$\boldsymbol{\Omega}=(D/\pi)[-(m-1)(s/[1-a^1])-(D/L)F_{(d)}-(mE/M)F_{(-b)}],$$
$$\Omega_{,1}=(D/\pi)[-(m-1)(s/[1-a^1])+(1/L)F_{(d)}-(m/M)F_{(-b)}],$$
$$\Omega_{,2}=(D/\pi)(G_{(d)}-mG_{(-b)}),$$
$$L^2=(1-D^2),\quad M^2=(1-E^2),$$
$$E=[(1+\sigma_s^2)D+2\sigma_s]/[1+\sigma_s^2+2\sigma_sD],$$
$$d=D/(1+L),\quad b=E/(1+M),$$
$$m=(1+D)(1+E)/(1-D)(1-E),$$
$$s^2=1-a^ia^i=1-r^2,$$
$$F_{(d)}=\frac{1}{2}\ln\frac{(1+Da^1)-sL}{(1+Da^1)+sL},$$
$$G_{(d)}=-\tan^{-1}\frac{(D+a^1)s}{(1+Da^1)a^2}-\tan^{-1}\frac{s}{a^2},$$
$$F_{(-b)}=\frac{1}{2}\ln\frac{(1-Ea^1)-sM}{(1-Ea^1)+sM},$$
$$G_{(-b)}=\tan^{-1}\frac{(E-a^1)s}{(1-Ea^1)a^2}-\tan^{-1}\frac{s}{a^2},$$
$$f_{(d)}=s-[(a^1+D)/L]F_{(d)}+a^2G_{(d)},$$
$$f_{(-b)}=s-[(a^1-E)/M]F_{(-b)}+a^2G_{(-b)}.$$

A further interesting point is that a second approximation may be readily carried out in the neighborhood of the reflected wave. This is done by developing the expressions for $F_{(d)}$ and $G_{(d)}$ above as a power series in s. The result for $f_{(d)}$ becomes $f_{(d)}=(1+D)s^3/3(1-a^1)(1+Da^1)$, and Ω becomes (in the neighborhood of $r=1$, $s=0$)

$$\Omega\approx\frac{D}{\pi}\frac{2(D+\sigma_s)(1+D\sigma_s)}{1+\sigma_s^2+2D\sigma_s}\frac{\sigma_s-a^1}{(1-a^1)(1+Da^1)(1-Ea^1)}\frac{s^3}{3},$$
$$\Omega\approx\frac{D}{\pi}\Delta(a^1)\frac{s^3}{3},\quad \Omega_{,i}\approx\frac{D}{\pi}sa^i\Delta(a^1),\quad \boldsymbol{\Omega}\approx\frac{D}{\pi}s\Delta(a^1).$$

The velocity potential now includes a second-order term which may be evaluated using the first-order solution above. The result of this procedure is that

$$r=1+\tfrac{1}{4}\delta^2(\gamma^2-1)[(D/\pi)\Delta(a^1)]^2,$$
$$p=p_B\{1+\delta^2\gamma(\gamma-1)[(D/\pi)\Delta(a^1)]^2\}$$

which indicates that the reflected shock is actually of variable strength, although even in this approximation the strength is zero for $a^1=\sigma_s$, at the triple point.

Contours of constant $\boldsymbol{\Omega}$, and hence constant density, may be drawn for various incident shock strengths. These contours are confined to the zeroth-order region, and some modification must be made to correspond with experiment where the observed region of variable density has the actual boundaries of Fig. 3. In a later section of this paper a correction will be made to permit more realistic comparison with experiment.

Figure 4 is an example of the contours resulting from this computation. In this case the shock strength is $p_B:p_A=1.25$; $\sigma_s=0.910$.

LIGHTHILL'S METHOD

Lighthill[5] has attacked a similar problem, but his treatment is sufficiently different to warrant summarizing here; the details are readily available in his original paper. The specific problem discussed is the diffraction of a shock wave at a convex corner; however, so far as an approximation including only first-order terms in the angle is concerned, this should give results comparable to those of Bargmann if the sign of the angle of the wall is taken into account. The reflected wave is not treated as a shock, and the boundary condition used is that the pressure be continuous at the boundary between the regions B and C of Fig. 3. In other words it is assumed that the "trivial" three-shock solution holds in the neighborhood of the triple point.

Lighthill has been able to avoid the assumption of isentropy in region C by choosing the pressure as the dependent variable to be isolated. This permits the relaxation of the restriction that the incident shock wave be weak. For sufficiently strong incident shocks, the flow in region B may be supersonic relative to the wall; i.e., in the coordinate system of Fig. 3 the wall may move to the left with a velocity which is greater than that of sound in region B. This results in the possibility of an attached shock wave at the corner and the situation becomes that of Fig. 5 in which the coordinate system is chosen in the same manner as that in Fig. 3.

Figure 5 illustrates a diffraction at a convex angle which gives, for the purposes of this treatment, a negative value of the angle φ and its tangent which has been called δ. The circular arc BCT is the locus of a sound signal which originated at the corner and is propagating into region B with the speed of sound.

[5] M. J. Lighthill, Proc. Roy. Soc. (London) **A198**, 454–470 (1949).

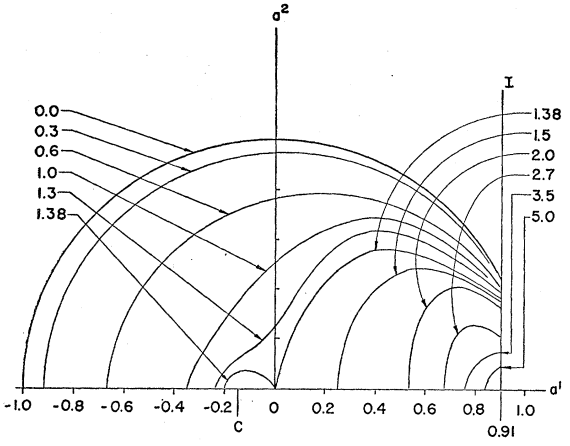

FIG. 4. Results of Bargmann's calculation of the density field. The contours are those of constant density (or pressure). The numbers associated with the contours are the values of the quantity $\Delta\rho/\delta$ or $\Delta p/\gamma\delta$ in the units used for this treatment. The incident shock has a pressure ratio $p_B:p_A=1.25:1$, $\sigma_s=0.91$.

The linearized pseudo-stationary treatment may be used, and the thermodynamic property that the density is a function of the pressure and entropy alone is used to relate the pressure and density:

$$\rho_{,i}=(\partial\rho/\partial p)_s p_{,i}+(\partial\rho/\partial S)_p S_{,i} \tag{60}$$

and

$$a^i\rho_{,i}=(1/c^2)a^i p_{,i}+(\partial\rho/\partial S)a^i S_{,i}; \tag{61}$$

but this last term vanishes according to Eq. (32), and the c^2 above may be replaced by $c_B{}^2=1$, since the term it multiplies is already first order in δ. When Eq. (61) is applied to region C, it becomes

$$\gamma a^i\Delta\rho_{,i}=a^i\Delta p_{,i}. \tag{62}$$

Equations (30), (31), and (62) may be combined to eliminate $\Delta\rho$ and u^i to give the single relation which Δp must satisfy:

$$\Delta p_{,ii}=2a^i\Delta p_{,i}+a^i a^j\Delta p_{,ij}. \tag{63}$$

This equation is identical with that for Ω which would be derived from Eq. (51) and the relation (49) between Ω and $\boldsymbol{\Omega}$.

The equation for Δp is elliptic within the region $BCTQB$, and it is at the boundaries of this region that the conditions on Δp or its derivatives must be supplied. These boundary conditions may be written down by referring to Eqs. (35) to (45).

The region ABC has a pressure which is attained by the gas passing through the linearized Prandtl-Meyer wave and is a region of uniform flow; hence, the pressure along the arc BC of the unit circle is given by

$$\Delta p=\gamma\delta D^2(D^2-1)^{-\frac{1}{2}} \quad \text{for} \quad D>1. \tag{64}$$

The pressure along the arc CT is given by

$$\Delta p=0. \tag{65}$$

This discontinuity in pressure at point C for the case that $D>1$ corresponds to the discontinuous boundary condition that arises at the corner A when it falls within the unit circle (see Fig. 3). The location of the point C is $a^1=-1/D$:

Along BOQ:

$$\Delta p_{,2}=0, \tag{66}$$

Along TQ: Equations (42) and (44) may be combined to give

$$\Delta p=2\gamma\sigma_s u^1[(\gamma-1)\sigma_s{}^2+2]/[(3\gamma-1)\sigma_s{}^2-(\gamma-3)] \tag{67}$$

and

$$\Delta p_{,2}=[4\gamma\sigma_s/(\gamma+1)D]a^2 u_{,2}{}^2 \tag{68}$$

from Eqs. (42) and (45) by differentiation with respect to a^2.

These may be combined with Eqs. (30) and (31) to give the relation,

$$\sigma_s[\sigma_s\Delta p_{,1}+a^2\Delta p_{,2}]=\Delta p_{,1}-\frac{(3\gamma-1)\sigma_s{}^2-(\gamma-3)}{2\sigma_s[(\gamma-1)\sigma_s{}^2+2]}a^2\Delta p_{,2}+\frac{(\gamma+1)D}{4a^2}\Delta p_{,2}, \tag{69}$$

by differentiating Eq. (67) with respect to a^2 and eliminating $u_{,1}{}^1$ and $u_{,2}{}^2$ from Eq. (30). This single relation between the derivatives of Δp along TQ may be supplemented by an integral relation by observing that at T, $u^2=0$ and at Q, $u^2=\delta D$, according to Eq. (36). Equation (68) may be integrated from the wall to above T to give the relation,

$$\int_Q^T[(\gamma+1)D/4\gamma\sigma_s a^2]\Delta p_{,2}da^2=\int_Q^T u_{,2}{}^2da^2=-\delta D; \tag{70}$$

hence,

$$[(\gamma+1)/4\gamma\sigma_s]\int_{a^2=0}^{a^2=\infty}d(\Delta p)/a^2=-\delta. \tag{71}$$

Lighthill then used the transformation used by Bargmann [Eq. (59)] to convert Eq. (63) to the laplace equation, which was then solved by a conformal transformation procedure. The results are available in Lighthill's paper referred to above.

Lighthill has calculated the pressure on the wall and the shape of the Mach shock. One point of special interest is that the ratio of the curvature of the Mach shock to δ has a maximum near the triple point, and this maximum approaches the triple point and becomes larger in magnitude as the strength of the incident shock increases. This indicates a region of rapidly changing entropy along the boundary of region C. The pressure along the wall is compared with experiment in the section on experimental results.

An addition could be made to this treatment which permits the calculation of the density to the first order.

The relation between the density and pressure increments for two points which have the same entropy is given by

$$\Delta p-\gamma\Delta\rho=\text{const.} \tag{72}$$

The constant may be evaluated by determining the place at the shock which has the same entropy as at the point in question. After unit time the point on the shock which has the same entropy as the particle located at (a^1, a^2) within the body of the fluid has the coordinates $(\sigma_s, a^2\sigma_s/a^1)$, since the shock configuration grows about the origin and to the zeroth order the fluid does not move. The density thus becomes

$$\gamma\Delta\rho(a^1, a^2)=\Delta p(a^1, a^2) -\frac{(1-\sigma_s^2)(\gamma-1)}{\sigma_s^2[(\gamma-1)\sigma_s^2+2]}\Delta p\left(\sigma_s, \frac{a^2\sigma_s}{a^1}\right). \tag{73}$$

The treatment Bargmann has used, which includes the assumption of isentropy in region C, requires that the contours of uniform density (isopycnals) and uniform pressure (isobars) which pass through any point must coincide along their whole length. According to Eq. (73) this not the case in the triangular region with vertices at OTQ.

THE METHOD OF TING AND LUDLOFF

Ting and Ludloff[6] have outlined a treatment which they have applied to the Mach reflection problem, but which they extended to treat the result when any thin airfoil is struck by a shock wave. The note referred to above is very brief and the discussion below is our own interpretation of the reasoning used.

The method used involves linearizing the differential equations for the flow including the time as an independent variable. If one employs the symbols and notation previously used and adds a subscript t to indicate differentiation with respect to the time, the linearized equations become

$$\Delta p,_t=-\gamma u,_i{}^i, \tag{74}$$

$$\Delta p,_i=-\gamma u,_t{}^i, \tag{75}$$

when $\Delta\rho$ has been eliminated according to the relation,

$$\Delta p,_t=\gamma\Delta\rho,_t. \tag{76}$$

The equation for Δp may be obtained by eliminating the derivatives of the u^i from these equations; this results in the wave equation as usual in acoustic theory. The boundary conditions are complicated by the fact that the incident shock is a boundary which is moving with velocity σ_s (in the coordinate system of Figs. 3 and 5). This moving boundary may be reduced to rest at the origin if the independent variables are subjected

[6] L. Ting and H. F. Ludloff, J. Aeronaut. Sci. **18**, 143 (1951).

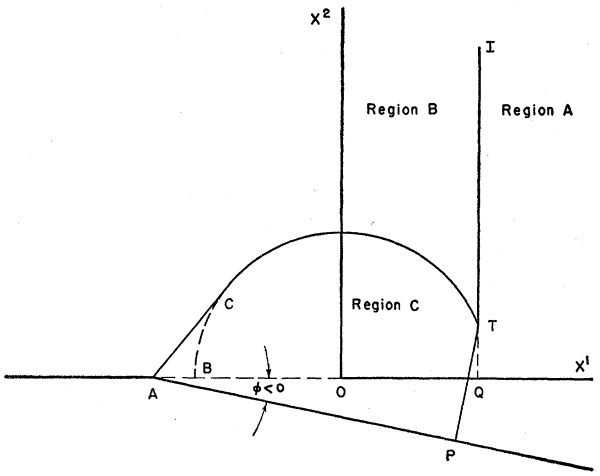

FIG. 5. The interaction of a strong incident shock I with a concave corner (nearly glancing incidence). The regions are similar to those of Fig. 3. The dashed curves are part of the zero-order boundary for Lighthill's calculation.

to a Lorentz transformation:

$$\begin{aligned}[x^1]&=(x^1-\sigma_s t)/(1-\sigma_s^2)^{\frac{1}{2}},\\ [x^2]&=x^2,\\ [t]&=(t-x^1\sigma_s)/(1-\sigma_s^2)^{\frac{1}{2}},\end{aligned} \tag{77}$$

since the units have been chosen to make the velocity of sound unity. The wave equation, of course, is invariant under a Lorentz transformation; hence, the equation to be solved is

$$\Delta p,_{[ii]}=\Delta p,_{[tt]}, \tag{78}$$

where the brackets enclosing the subscripts indicate that the transformed variables are meant.

In the coordinate system of Fig. 3, the airfoil surface is given by the equation,

$$x^2=f(x^1+Dt), \tag{79}$$

and after the Lorentz transformation this becomes

$$[x^2]=f\left\{\frac{1+D\sigma_s}{(1-\sigma_s^2)^{\frac{1}{2}}}([x^1]+[D][t])\right\},\quad [D]=\frac{D+\sigma_s}{1+D\sigma_s}. \tag{80}$$

In the case of interaction with a wedge, one obtains

$$f(x^1+Dt)=\begin{cases}(x^1+Dt)\delta & x^1>-Dt\\ 0 & x^1<-Dt\end{cases}. \tag{81}$$

The condition that the flow follow the airfoil surface may be written

$$\begin{aligned}u^2&=Df'(x^1+Dt),\\ u,_t{}^2&=D^2f''(x^1+Dt),\end{aligned} \tag{82}$$

from Eq. (75). The condition on the derivative of the pressure is thus

$$\Delta p,_2=-\gamma D^2f''(x^1+Dt). \tag{83}$$

In the case of the infinite wedge of angle φ, this condition may be written (see Eq. (38))

$$\Delta p,_2 = -\delta\gamma D^2[\text{delta-function of } (x^1+Dt)]. \quad (84)$$

When this condition is applied to an airfoil, care must be taken to include a delta-function with suitable multiplier at each point that the f' defined above has a discontinuity.

The conditions at the shock wave which are expressed in Eqs. (42) to (45) for the pseudo-stationary case may be written in the form,

$$\Delta p = (4\gamma\sigma_s/[\gamma+1])f_{(1),t}, \quad (85)$$

$$u^1 = \frac{2}{\gamma+1}\left[\frac{(3\gamma-1)\sigma_s^2-(\gamma-3)}{(\gamma-1)\sigma_s^2+2}\right]f_{(1),t}, \quad (86)$$

$$u^2 = -Df_{(1),2}, \quad (87)$$

which must hold at $x^1=\sigma_s t$. By applying the Lorentz transformation and eliminating carefully by differentiation with respect to $[x^2]$ and $[t]$, one may obtain the following condition:

$$D_{[1,t]}{}^{(2)}\Delta p = \Delta p,_{[11]} + 2\sigma_s\Delta p,_{[1t]} + (1/M_1{}^2)\Delta p,_{[tt]} = 0, \quad (88)$$

where

$$M_1{}^2 = [(\gamma-1)\sigma_s{}^2+2]/[2\gamma\sigma_s{}^2-(\gamma-1)].$$

This may be written

$$\left(\frac{\partial}{\partial[x^1]}+a\frac{\partial}{\partial[t]}\right)\left(\frac{\partial}{\partial[x^1]}+b\frac{\partial}{\partial[t]}\right)\Delta p = 0, \quad (88')$$

where

$$a = \sigma_s+(\sigma_s{}^2-1/M_1{}^2)^{\frac{1}{2}},$$

$$b = \sigma_s-(\sigma_s{}^2-1/M_1{}^2)^{\frac{1}{2}},$$

which must hold at $[x^1]=0$; and $D_{[1,t]}{}^{(2)}$ represents the second-order differential operator which is defined by Eq. (88). This equation is equivalent to the conditions Eqs. (85–87) in view of the equations of motion Eqs. (74–75).

The solution of the wave equation is carried out by a modification of Volterra's method which has been used by several workers in aerodynamics.[7,8] This method is based on applying a form of Green's theorem in the following way:

$$\int_V (v\Box\Delta p - \Delta p\Box v)dV = \int_S [v(\partial\Delta p/\partial\nu)-\Delta p\partial v/\partial\nu]dS, \quad (89)$$

where the symbol $\Box$ represents the operator

$$(\partial^2/\partial[x^1]^2)+(\partial^2/\partial[x^2]^2)-\partial^2/\partial[t]^2 \quad (90)$$

and the derivative $\partial/\partial\nu$ is the derivative along the co-normal to the surface. The volume V is chosen as a right circular Mach cone with its vertex at the point $[x^1]=\xi$, $[x^2]=\eta$, $[t]=\tau$, at which Δp is to be evaluated and having a base at $[t]=-T$, $T>0$, from which certain sections are excluded. In particular, an infinitesimal cylinder surrounding the axis is excluded, as is an infinitesimal section surrounding the portion of the $[x^2]=0$ plane which is inside the cone. The function v is chosen to be

$$v = \ln\frac{(\tau-[t])+\{(\tau-[t])^2-(\xi-[x^1])^2-(\eta-[x^2])^2\}^{\frac{1}{2}}}{\{(\xi-[x^1])^2+(\eta-[x^2])^2\}^{\frac{1}{2}}}, \quad (91)$$

which satisfies the equation $\Box v=0$ within the cone and $v=0$ on its surface. Since v is a constant on the surface of the cone, $\partial v/\partial\nu$ is zero there because the co-normal is parallel to the surface. The function v is singular along the axis of the cone. The quantity Δp satisfies the equation $\Box\Delta p=0$ everywhere except at the plane $[x^2]=0$. It is further postulated that Δp is singular at this plane by the circumstance that its normal derivative at $[x^2]=0$ is discontinuous:

$$\Delta p,_{[2]}([x^2]\to 0^-) = -\Delta p,_{[2]}([x^2]\to 0^+). \quad (92)$$

This corresponds to a layer of "single sources" on $[x^2]=0$.

The region of physical interest (regions B and C of Fig. 3) now are delimited by the conditions that $\xi\leqslant 0$; η, $\tau\geqslant 0$. By considering the portion of the right circular cone with $[x^2]<0$ and the base given above and applying Eq. (89), one can easily see that

$$v\Delta p,_{[2]} = \Delta p v,_{[2]}([x^2]\to 0^-), \quad (93)$$

since Δp and its derivatives are zero on the base which represents conditions at a time before the shock struck the wedge.

This information along with the postulate Eq. (92) permits evaluation over the part of the cone with $[x^2]>0$. Since both v and Δp are solutions of the wave equation, the left-hand side of Eq. (89) vanishes. The integral over the lateral surface of the cone and its base are zero, since on the former v and $\partial v/\partial\nu$ are zero, whereas over the latter Δp and its derivative are zero. The limit of the surface integral over the infinitesimal cylinder is

$$2\pi\int_{-T}^{\tau}\Delta p(\xi,\eta,[t])d[t], \quad (94)$$

and the integral over the surface near $[x^2]=0$ is given by

$$2\int\int_H v([x^1],0,[t])\Delta p,_{[2]}([x^1],0,[t])d[x^1]d[t]; \quad (95)$$

[7] C. S. Gardner and H. F. Ludloff, J. Aeronaut. Sci. **17**, 47–59 (1950).

[8] I. E. Garrick and S. I. Rubinow, NACA Technical Note No. 1383 (1947).

thus one obtains

$$\int_{-T}^{\tau}\Delta p(\xi,\eta,[t])d[t]=-\frac{1}{\pi}\int\int_{H}\Delta p_{,[2]}([x^1],0,[t])\times\ln\frac{(\tau-[t])+\{(\tau-[t])^2-(\xi-[x^1])^2-\eta^2\}^{\frac{1}{2}}}{[(\xi-[x^1])^2-\eta^2]^{\frac{1}{2}}}. \quad (96)$$

The area of integration is the hyberbola in the $[x^2]=0$ plane, which is the intersection of the plane $[x^2]=0$ with the cone. If this equation is differentiated with respect to τ, taking into account that this variation in τ varies the hyperbola as well, it follows that

$$\Delta p(\xi,\eta,\tau)=-\frac{1}{\pi}\int\int_{H}\frac{\Delta p_{,[2]}([x^1],0,[t])d[x^1]d[t]}{[(\tau-[t])^2-(\xi-[x^1])^2-\eta^2]^{\frac{1}{2}}}. \quad (97)$$

This gives the basis of the method, but it takes no account of the conditions along the Mach shock which are conditions on Δp at $\xi=0$. Ting and Ludloff translate these into conditions on $\Delta p_{,[2]}$ in the plane $[x^2]=0$. It may be readily shown that

$$\Delta p_{,\xi\xi}=-\frac{1}{\pi}\int\int_{H}\frac{\Delta p_{,[211]}([x^1],0,[t])d[x^1]d[t]}{[(\tau-[t])^2-(\xi-[x^1])^2-\eta^2]^{\frac{1}{2}}} \quad (98)$$

by performing the differentiation of the integral, taking into account the dependence of the limits of integration on ξ and noticing that

$$(\partial/\partial\xi)[(\tau-[t])^2-(\xi-[x^1])^2-\eta^2]^{-\frac{1}{2}}=-(\partial/\partial[x^1])[(\tau-[t])^2-(\xi-[x^1])^2-\eta^2]^{-\frac{1}{2}}. \quad (99)$$

Integration by parts then gives the results of Eq. (98). Similar relations hold for $\Delta p_{,\xi\tau}$ and $\Delta p_{,\tau\tau}$. The shock condition then is

$$D_{\xi\tau}{}^{(2)}\Delta p(0,\eta,\tau)=-\frac{1}{\pi}\int\int_{H}\frac{D_{[1t]}{}^{(2)}\Delta p_{,[2]}([x^1],0,[t])d[x^1]d[t]}{\{(\tau-[t])^2-[x^1]^2-\eta^2\}^{\frac{1}{2}}}. \quad (100)$$

According to the conditions of the problem, $\Delta p_{,[2]}([x^1],0,[t])$ is defined only for $[x^1]<0$, i.e., behind the incident shock. It is possible to define this quantity for positive values of $[x^1]$ in such a manner that the shock condition is automatically satisfied. This is accomplished by requiring that

$$D_{[1t]}{}^{(2)}\Delta p_{,[2]}([x^1],0,[t])=-D_{[1t]}{}^{(2)}\Delta p_{,[2]}(-[x^1],0,[t]);\ [x^1]>0. \quad (101)$$

If $\Delta p_{,[2]}([x^1],0,[t])$ satisfies Eq. (101), then the Δp calculated according to Eq. (97) will satisfy the condition given by Eq. (88) and hence the conditions Eqs. (85–87).

The right-hand side of Eq. (101) is a known function of $[x^1]$ and $[t]$ determined by Eq. (83) and $D_{[1t]}{}^{(2)}$. The solution of Eq. (101) is

$$\Delta p_{,[2]}([x^1],0,[t])=F([t]-a[x^1])+G([t]-b[x^1])+Bf''\left\{\frac{1+D\sigma_s}{(1-\sigma_s^2)^{\frac{1}{2}}}([D][t]-[x^1])\right\}, \quad (102)$$

where F and G are arbitrary functions of their arguments and the quantities a and b are defined in Eq. (88′). These functions are evaluated by the requirement that $\Delta p_{,[2]}$ and $\Delta p_{,[21]}$ be continuous across the line $[x^1]=0$ in the plane $[x^2]=0$. This was assumed in deriving Eq. (98). It may be verified that

$$B=-\frac{M_1^2+2\sigma_sM_1^2[D]+[D]^2}{M_1^2-2\sigma_sM_1^2[D]+[D]^2},$$

$$F([t]-a[x])=\frac{B([D]b-1)-([D]b+1)}{[D](a-b)}\times f''\left\{\frac{D+\sigma_s}{(1-\sigma_s^2)^{\frac{1}{2}}}([t]-a[x^1])\right\},$$

$$G([t]-b[x])=\frac{B(1-[D]a)+(1+[D]a)}{[D](a-b)}\times f''\left\{\frac{D+\sigma_s}{(1-\sigma_s^2)^{\frac{1}{2}}}([t]-b[x^1])\right\}.$$

In the case that the obstacle is an infinite wedge and $f(x+Dt)$ is given by Eq. (81), the results for $\Delta p(x,y,t)$ may be written

$$\Delta p(x^1,x^2,t)=\sum_{j=1}^{4}A_j\cos^{-1}\frac{(t+\alpha_jx^1)}{(\alpha_jt+x^1)^2-(\alpha_j^2-1)(x^2)^2}$$

if $D>1$, or in the event that $D<1$

$$\Delta p(x^1,x^2,t)=\sum_{j=1}^{2}A_j'\cosh^{-1}\frac{t+\alpha_jx^1}{(\alpha_jt+x^1)^2-(\alpha_j^2-1)(x^2)^2}+\sum_{j=3}^{4}A_j\cos^{-1}\frac{t+\alpha_jx^1}{(\alpha_jt+x^1)^2-(\alpha_j-1)(x^2)^2},$$

where

$$A_1=\gamma D^2\delta/\pi(D^2-1)^{\frac{1}{2}},\quad A_2=BA_1,$$

$$A_3=-(\gamma\delta D^2)\frac{B([D]b-1)-([D]b+1)}{[D](a-b)}\times\frac{(1-\sigma_s^2)^{\frac{1}{2}}}{\pi(D+\sigma_s)(1-a^2)^{\frac{1}{2}}},$$

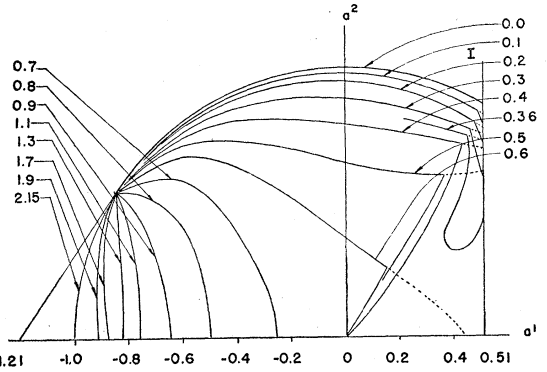

FIG. 6. Results of the calculation of the density field according to Ting and Ludloff. The solid lines are contours of constant density, the dashed lines indicate where the contours of constant pressure differ from the isopycnals. The numbers associated with the contours are $\Delta\rho/\delta$ for the isopycnals and $\Delta p/\gamma\delta$ for the isobars in the units used for this treatment. The incident shock has a pressure ratio $p_B:p_A=7.33:1$, $\sigma_s=0.51$.

$$A_4=-(\gamma\delta D^2)\frac{B(1-[D]a)+(1+[D]a)}{[D](a-b)}\times\frac{(1-\sigma_s^2)^{\frac{1}{2}}}{\pi(D+\sigma_s)(1-b^2)^{\frac{1}{2}}},$$

$$A_1'=-\gamma\delta D^2/\pi(1-D^2)^{\frac{1}{2}},\quad A_2'=BA_1'$$

$$\alpha_1=D,\quad \alpha_2=-[2\sigma_s+D(1+\sigma_s^2)]/[2D\sigma_s+(1+\sigma_s^2)],$$

$$\alpha_3=-(1+\sigma_s a)/[a+\sigma_s],\quad \alpha_4=-(1+\sigma_s b)/[b+\sigma_s].$$

The pressure in the region ABC of Fig. 5 is uniform and has the value given by

$$\Delta p=\gamma\delta D^2(D^2-1)^{-\frac{1}{2}}.$$

The density may be calculated by a scheme similar to that of Eq. (73):

$$\gamma\Delta\rho(x^1,x^2,t)=\Delta p(x^1,x^2,t)-\frac{(1-\sigma_s^2)(\gamma-1)}{\sigma_s^2[(\gamma-1)\sigma_s^2+2]}\Delta p\left(x^1,x^2,\frac{x^1}{\sigma_s}\right).$$

Figure 6 is a plot of the contours which result when the above calculation is carried out. The shock strength in this case is given by $p_B:p_A=7.33:1$. The solid lines represent contours of constant density; and in the region where the isopycnals and the isobars do not coincide, the latter are indicated by dashed lines.

EXPERIMENTAL RESULTS

A program of experimental work has been undertaken to investigate how closely these approximate treatments represent the actual interaction of a shock wave with a finite corner. This experimental program includes making quantitative measurements of the density field resulting from such interactions. Preliminary investigations[1,9] had already shown a qualitative resemblance to Bargmann's contours (Fig. 4).

Plane shock waves were generated in a shock tube[9] and made to pass over both convex and concave corners. The resultant density field was measured interferometrically. When qualitative results were desired, the interferometer was adjusted so that the illumination over the whole field of the interferometer was uniform. With this adjustment the contours of uniform photographic density correspond to contours of uniform gas density.

This technique was used in the series of interferograms in Figs. 7(a) to 7(f). In each of these pictures, the incident shock wave had a pressure ratio $p_B:p_A=1.25$ with $p_A=$ one atmosphere. The angle α was varied from 45° in Fig. 7(a) to 85° in Fig. 7(f) in the steps indicated.

Figure 7(a) shows a case of regular reflection; note that the signal from the corner is lagging behind the shock intersection, showing that if the shock intersection is considered at rest, the flow behind the reflected shock is supersonic. The conjectures of the Introduction regarding the straightness of the reflected shock and the uniformity of the density field in the neighborhood of the intersection are apparently verified.

Figure 7(b) shows the resultant field when the angle between the shock and the wall (α) is 60°. This is a typical Mach reflection pattern. Particular attention should be given to the discontinuity in the field behind the reflected and Mach shocks. This has been identified (tentatively) as the slipstream required by the three-shock theory. The angle ω corresponding to this picture falls in the region which is forbidden in the three-shock theory as presented in the Introduction.

Figures 7(c) and 7(d) show the fields which result when the angle is 65° and 70°, respectively. This series is not taken at a constant distance from the corner; hence, no comparison of the height of the Mach stem from picture to picture should be made. A measure of this growth is shown in Table I, which shows the values of α, χ, and ω which correspond to these pictures.

Figures 7(e) and 7(f) show the case that $\alpha=75°$ and 85°, respectively. The case of $\alpha=80°$ will be compared in detail below and is not included in this series. What should be noticed here is that apparently the slipstream has disappeared on increasing α from 70° to 75°.

The value $\alpha=80°$ was chosen for careful study because it provides a reasonable number of density contours to compare with theory, but still gives only a small effect on the flow. By using an interferogram with narrow parallel fringes it is possible to evaluate the actual density at various points in the field. It is found in this way that the density at the foot of the Mach stem as measured corresponds to that calculated by Bargmann's treatment for the density at the point Q (Fig. 3). In order to bring this point into the actual physical field an arbitrary crowding of the theoretical field was made. This compression involved modifying

[9] Bleakney, Weimer, and Fletcher, Rev. Sci. Instr. **20**, 807–815 (1949).

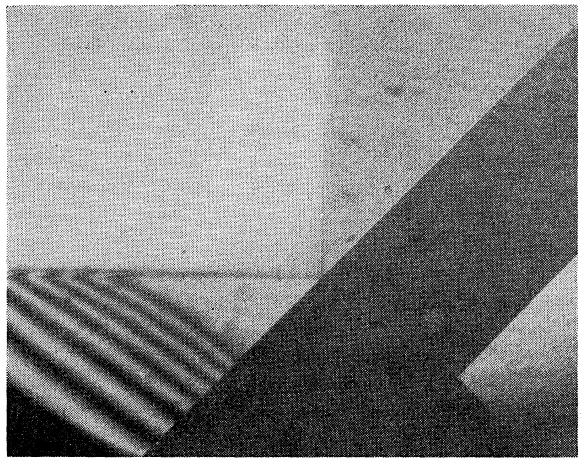

(a)

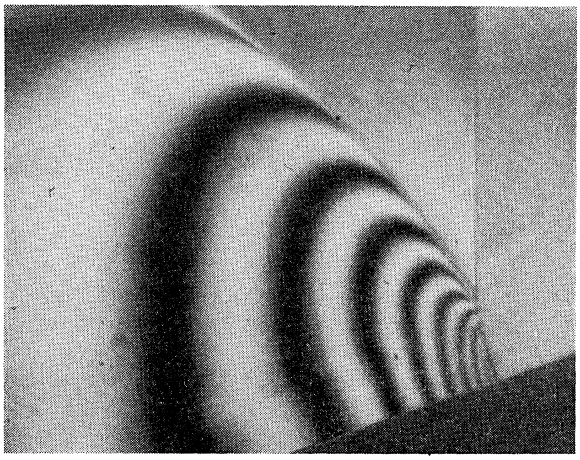

(d)

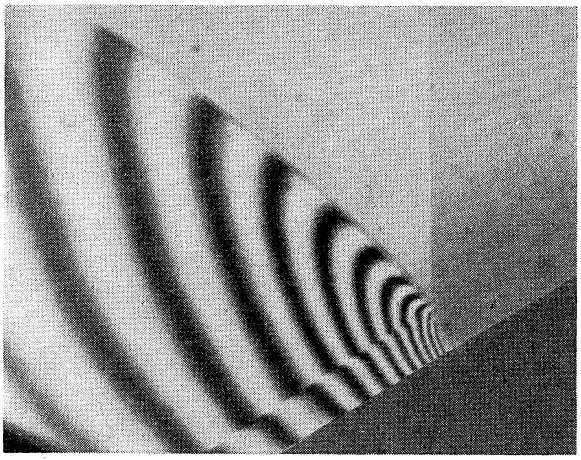

(b)

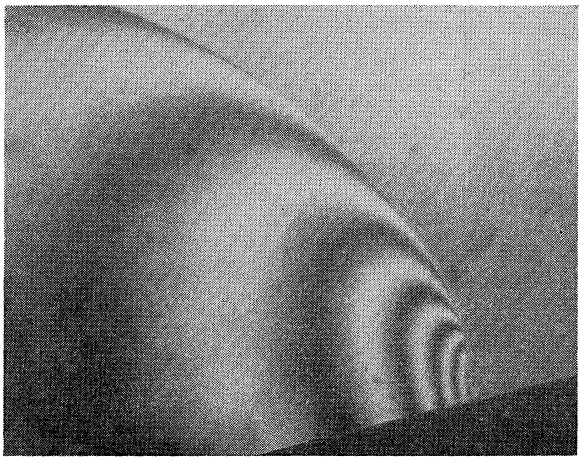

(e)

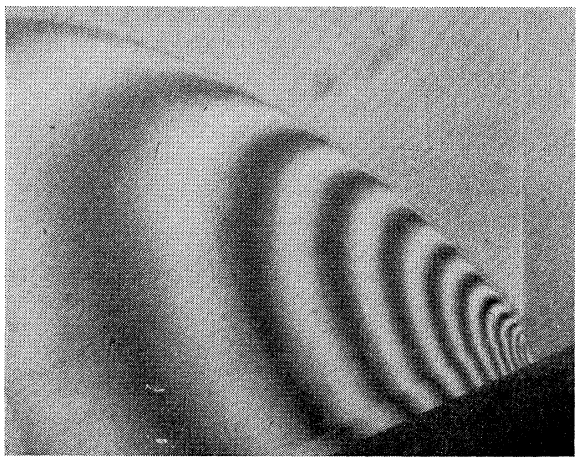

(c)

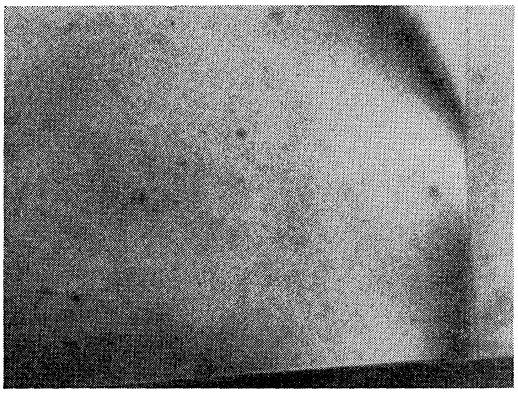

(f)

FIG. 7. Interferograms showing the density contours in the interaction of a weak shock with a wall at various angles of incidence. In all of these pictures the incident shock is traveling to the right and the interferometer has been adjusted so that in the undisturbed gas the whole field would be uniformly illuminated (single fringe adjustment). The strength of the incident shock is $p_B:p_A=1.25:1$. (a) $\alpha \parallel 45°$, (b) $\alpha=60°$, (c) $\alpha=65°$, (d) $\alpha=70°$, (e) $\alpha=75°$, (f) $\alpha=85°$.

TABLE I.

α	x	ω
60°	1°10′	58°50′
65°	2°40′	62°20′
70°	4°50′	65°10′
75°	6°50′	68°10′
80°	11°20′	68°40′

the calculated density contours as follows: contours of constant density were calculated for various values of the density, the compressed field was then obtained by leaving the reflected shock unaltered and compressing the distance along an ordinate between any contour and the reflected shock in the ratio of the distance of the reflected shock from the x^1 axis to the distance of the reflected shock from the reflecting surface. This is in the nature of a partial second approximation; it cannot be correct, for it has two flaws—there are still no contours in the region between P' and P, and the density contours are no longer normal to the wall, which they must be according to the assumptions made in deriving the boundary conditions.

Figure 8 shows the actual density field with the Bargmann contours which correspond to integral fringe shifts from the region ahead of the incident shock drawn in after having been adjusted according to the above scheme. It should be noted that a contour of constant *integral* fringe shift is determined in the interferogram by locating a curve of constant photographic density the same density as appears ahead of the incident shock. The dashed lines are the theoretically predicted positions of the shocks. The agreement of these positions is good. The fringe shift across the incident shock is known to be 10.2 fringes from a narrow fringe interferogram, and from measurement of the angle between the Mach and incident shock it may be calculated that the reflected shock is very weak at the triple point. Thus, the contour of maximum blackness just below the triple point is 10.5 fringes (from the region ahead of the incident shock), and the region of least blackness next below is 11 fringes, corresponding well with the theoretical fringe number 11 which is drawn there. Once this is established, the contours progress downward as the fringe shift increases. As will be shown below, where the pressures on the wall are compared, the calculated and measured pressures at the foot of the Mach stem are in good agreement. Away from the Mach shock the contours agree only in their shape; this may be due in part to a slight maladjustment of the interferometer, but is more probably due to the finite angle of the wedge.

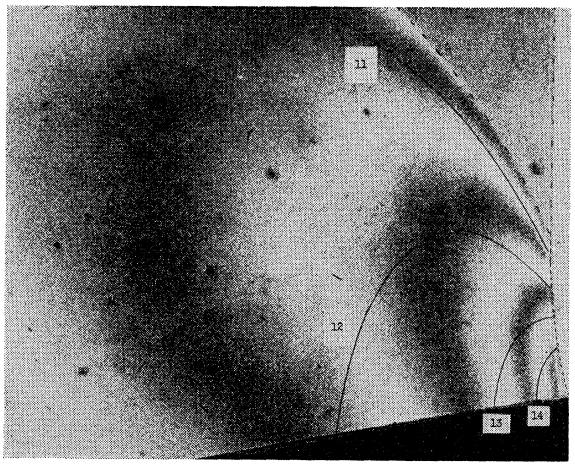

FIG. 8. Comparison of the single-fringe interferogram for $\alpha=80°$ with the predicted contours according to Bargmann's treatment as corrected for the finite angle $\varphi=10°$. The incident shock strength is given by $p_B:p_A=1.25:1$. The numbered contours are those calculated to represent the indicated fringe shift from the region ahead of the incident shock. The calculated position of the Mach and reflected shocks is indicated by dashed lines.

There are other points which may be compared with these theories. The position of the triple point is predicted; and the value of ω which corresponds to this location of the triple point is $\omega=68°50'$, which may be compared with Table I. The agreement here is good even for $\alpha=80°$.

As has been mentioned, Bargmann's second approximation gives a reflected shock of nonvanishing strength (away from the triple point). This reflected shock should have a maximum near the triple point. Figure 9 shows a narrow fringe interferogram of the vicinity of the triple point. The reflected wave appears to have a rather broad maximum in fringe shift across it somewhere near the center of the field shown, but this aspect of the problem requires further investigation.

The pressure along the wall was compared with Lighthill's curves for a slightly stronger shock.[10] In this case the pressure ratio across the incident shock was 2:1, and the angles used were 0.1 radian both convex and concave. The results are plotted in Fig. 10. The ordinate is the reduced pressure excess as used by Lighthill (modified to accommodate the sign change for δ) $P=(p-p_B)/\delta(p_B-p_A)$, and the abscissa is the distance measured along the wall from the corner with the distance to the undisturbed incident shock set equal to unity. The vertical length of the line segments is a measure of the experimental error in the measurements. The plain line segment represents $\varphi=+0.1$ radian (a concave corner), whereas the crossed line segment represents a convex corner of the same magnitude. Note that the case of the concave corner near the abscissa 1 lies below the theoretical curve. This is the result of the fact that the foot of the Mach shock has advanced ahead of the location of the incident shock. This is qualitatively the same situation as shown on the comparison of the contours, Fig. 8.

There is one further comparison which has been made by D. R. White.[11] Figure 11 is a preliminary drawing that gives the density contours which result when a

[10] Fletcher, Weimer, and Bleakney, Phys. Rev. **78**, 634 (1950).
[11] D. R. White, thesis, Princeton University, May, 1951 and J. Aeronaut. Sci. **18**, 633 (1951).

strong shock is reflected at a small angle wedge. This is to be compared with the contours calculated by Ting and Ludloff, given in Fig. 6. The shock strength has been chosen to correspond; but the wedge angle used in the experiment is such that the shock near the nose is curved instead of straight, as one would expect for an infinitesimal angle. By the nature of the experiment the shape of White's contours is more reliable than the absolute values of the density attached to them. Considering the departure of the experimental conditions from the ideal ones of the analysis and the experimental uncertainties involved, one cannot say that there is any conflict here between theory and observation.

SUMMARY

In this section we shall try to compare the three approximate treatments outlined in the body of this paper. All three of these dealt with the problem of almost glancing incidence of a plane shock on an obstacle.

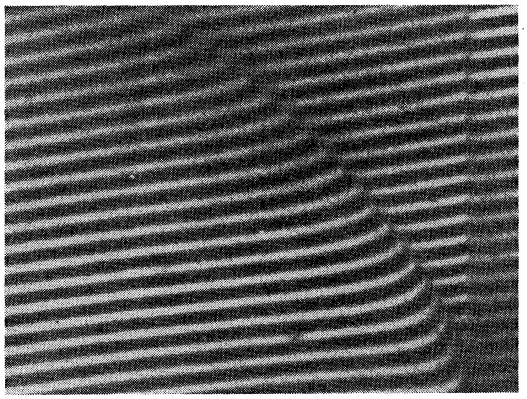

FIG. 9. A narrow fringe interferogram of the region near the triple point for the same shock conditions as those of Fig. 8. Note that there is an indication of a maximum in the fringe shift across the reflected shock and that the fringe shift seems to approach zero as the triple point is approached.

They used the slope of the obstacle as a parameter whose square could be neglected with respect to the first power and thus linearized the differential equation and the boundary conditions describing the phenomenon. Any physical quantity F was written as $F=F_0+\delta F_1$, and only first-order terms in δ were considered.

In linearizing the boundary conditions, it was found that the physical variables could be evaluated along curves different from the actual shocks and walls. These curves will be called the "zero-order boundaries." All three authors used as part of the zero-order boundaries the "trivial" three shock configuration mentioned in the Introduction. They either assumed initially or deduced that on the reflected shock $\Delta p=0$. Thus, in the neighborhood of the triple point these first-order solutions also correspond to the "trivial" three-shock configuration. Bargmann showed in addition that, even

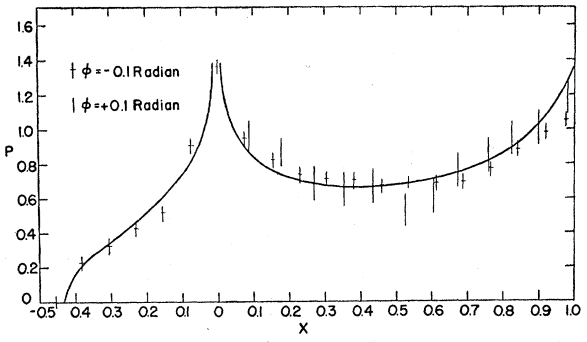

FIG. 10. Relative pressure excess $P=(p-p_B)/\delta(p_B-p_A)$ as a function of position along the wall. The corner is at the origin and the position of the incident shock at abscissa 1. The solid curve is that calculated by Lighthill for $p_B:p_A=2:1$. The experimental points were measured interferometrically for the angle $\varphi=\pm 0.1$ radian. The vertical height of the experimental point is an indication of the experimental error involved. The crossed symbol represents diffraction at a convex corner and the plain symbol represents interaction with a concave corner.

including second-order terms in the slope of the wall, $\Delta p=0$ at the reflected shock near the triple point.

Bargmann restricted himself to the case of weak incident shocks and thus was justified in assuming irrotationality (and isentropy) of the pseudo-stationary flow he considered. He used as a primary dependent variable the velocity potential and formulated the boundary conditions in terms of this variable. He made use of the weakness of the incident shock to simplify the resulting equations. He was able to determine the isobars and the shape of the Mach shock to first approximation. In addition to showing that $\Delta p=0$ even in the second approximation on the reflected shock near the triple point he showed that the gradient of Δp had a singularity in the second approximation in the vicinity of this point.

Lighthill also considered a pseudo-stationary flow, but used the pressure as the primary dependent variable. He formulated the boundary conditions in terms of this variable. The differential equation satisfied by the pres-

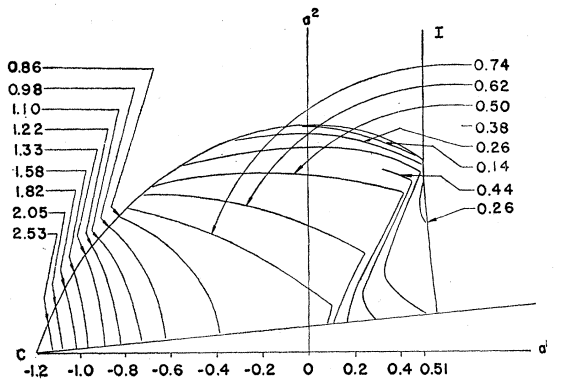

FIG. 11. Constant density contours drawn from an interferometric investigation of the situation calculated by Ting and Ludloff. This is to be compared with Fig. 6. The numbers associated with the contours represent the quantity $\Delta\rho/\delta$ as in Fig. 6.

sure turns out to be identical with that satisfied by Bargmann's velocity potential in a suitably chosen coordinate system. By using the pressure as the primary variable, Lighthill was able to free himself from the assumption of weak incident shocks. He paid particular attention to calculating the pressure on the reflecting wall and to the curvature of the Mach shock.

Ting and Ludloff also used the pressure as a primary variable. However, they did not restrict themselves to pseudo-stationary flows; and as a consequence, they can treat a sharp obstacle of arbitrary shape. They have calculated the isobars and isopycnals and have called attention to the discontinuity in the slope of the latter. This discontinuity, however, does not correspond exactly to the slipstream observed experimentally.

Experimental evidence indicates that the observed slipstreams are in fact discontinuities in the density itself. Such slipstreams are found experimentally in the reflection of any shock at suitable angles; these angles are not in the region of near glancing incidence. For the case of strong incident shocks, there is agreement between the observed shock configuration and that required by the local three shock theory (see Introduction). That theory requires a discontinuity in density which is observed. The slipstream in the case of weak incident shocks where the configuration is in violation of the local three shock theory (see Fig. 7(b)) seems experimentally to be a sharp density discontinuity. One can infer from Lighthill's analysis that a calculation similar to that of Ting and Ludloff, but for weak shocks, would show a broad region of changing density.

It is evident that although the results of these approximate treatments are very interesting and deal with the problem of glancing incidence adequately, the fundamental problem of Mach reflection of weak shocks is not yet solved.

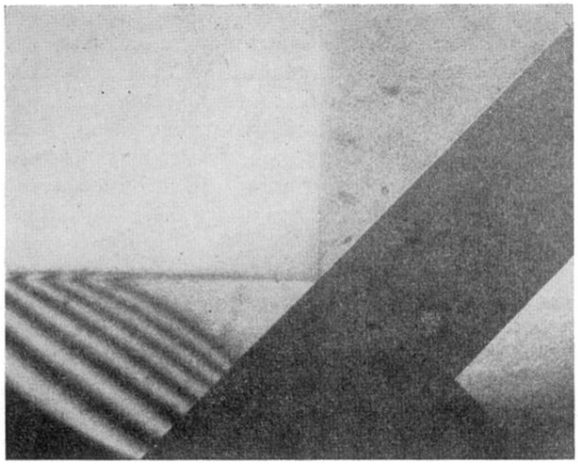

(a)

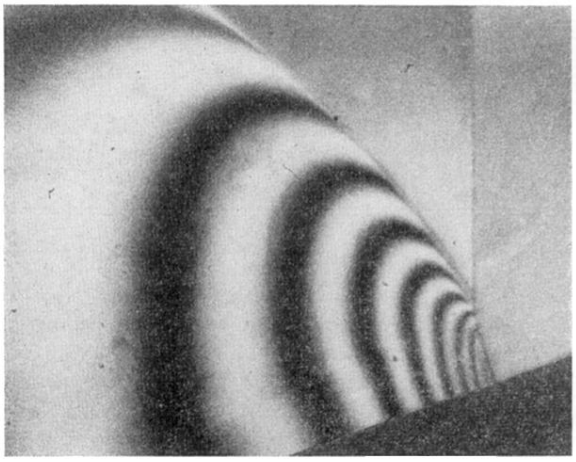

(d)

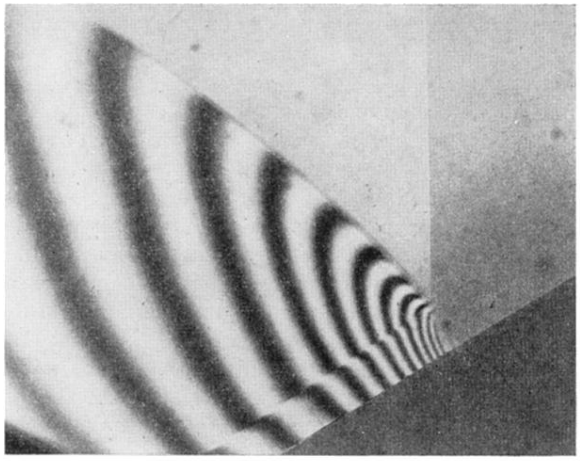

(b)

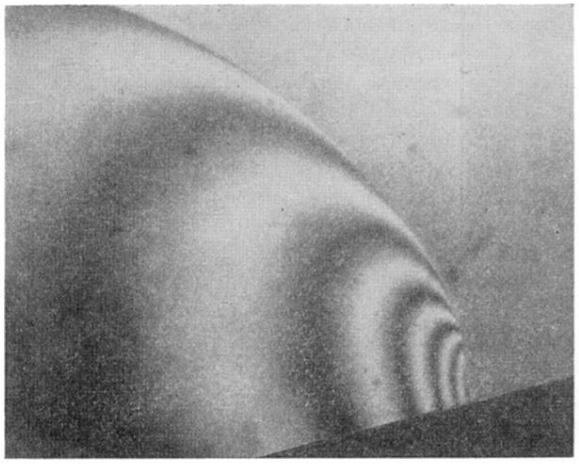

(e)

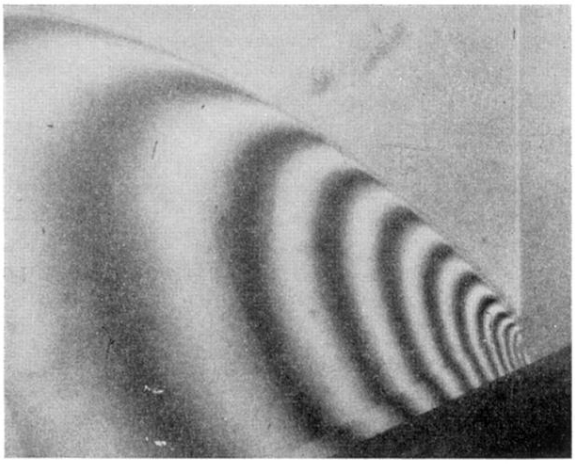

(c)

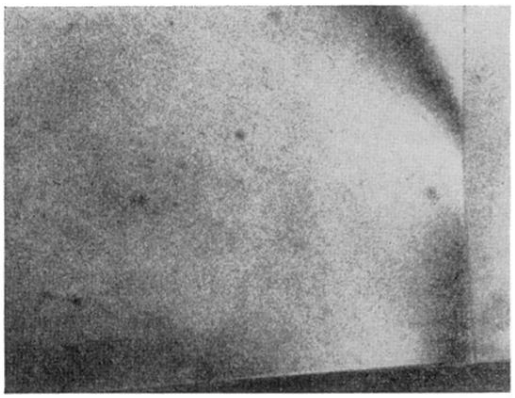

(f)

FIG. 7. Interferograms showing the density contours in the interaction of a weak shock with a wall at various angles of incidence. In all of these pictures the incident shock is traveling to the right and the interferometer has been adjusted so that in the undisturbed gas the whole field would be uniformly illuminated (single fringe adjustment). The strength of the incident shock is $p_B : p_A = 1.25 : 1$. (a) $\alpha \parallel 45°$, (b) $\alpha = 60°$, (c) $\alpha = 65°$, (d) $\alpha = 70°$, (e) $\alpha = 75°$, (f) $\alpha = 85°$.

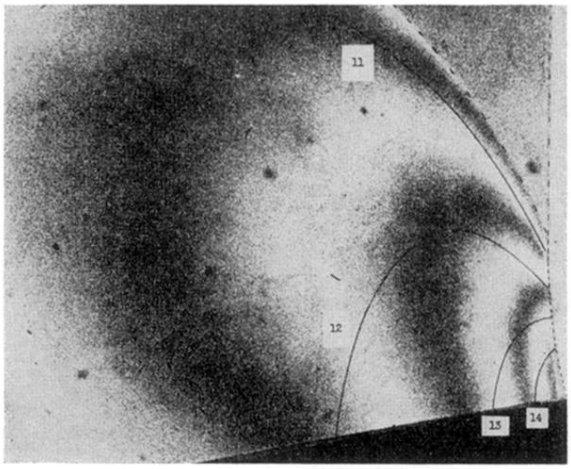

FIG. 8. Comparison of the single-fringe interferogram for $\alpha=80°$ with the predicted contours according to Bargmann's treatment as corrected for the finite angle $\varphi=10°$. The incident shock strength is given by $p_B:p_A=1.25:1$. The numbered contours are those calculated to represent the indicated fringe shift from the region ahead of the incident shock. The calculated position of the Mach and reflected shocks is indicated by dashed lines.

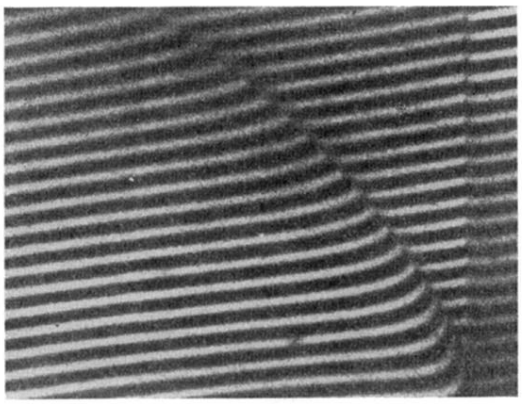

FIG. 9. A narrow fringe interferogram of the region near the triple point for the same shock conditions as those of Fig. 8. Note that there is an indication of a maximum in the fringe shift across the reflected shock and that the fringe shift seems to approach zero as the triple point is approached.